frontiers | Frontiers in Nutrition

TYPE Original Research
PUBLISHED 15 September 2022
DOI 10.3389/fnut.2022.992502

Check for updates

OPEN ACCESS

EDITED BY
Peng Ji,
Gansu Agricultural University, China

REVIEWED BY
Xiaofei Shang,
Lanzhou Institute of Husbandry and Pharmaceutical Sciences (CAAS), China
Guangliang Shi,
Northeast Agricultural University, China

*CORRESPONDENCE
Jingui Li
jgli@yzu.edu.cn
Huan Pang
panghuan@yzu.edu.cn

†These authors have contributed equally to this work

SPECIALTY SECTION
This article was submitted to Nutritional Immunology, a section of the journal Frontiers in Nutrition

RECEIVED 12 July 2022
ACCEPTED 29 August 2022
PUBLISHED 15 September 2022

CITATION
Bo R, Liu X, Wang J, Wei S, Wu X, Tao Y, Xu S, Liu M, Li J and Pang H (2022) Polysaccharide from *Atractylodes macrocephala* Koidz binding with zinc oxide nanoparticles: Characterization, immunological effect and mechanism. *Front. Nutr.* 9:992502. doi: 10.3389/fnut.2022.992502

COPYRIGHT
© 2022 Bo, Liu, Wang, Wei, Wu, Tao, Xu, Liu, Li and Pang. This is an open-access article distributed under the terms of the Creative Commons Attribution License (CC BY). The use, distribution or reproduction in other forums is permitted, provided the original author(s) and the copyright owner(s) are credited and that the original publication in this journal is cited, in accordance with accepted academic practice. No use, distribution or reproduction is permitted which does not comply with these terms.

Polysaccharide from *Atractylodes macrocephala* Koidz binding with zinc oxide nanoparticles: Characterization, immunological effect and mechanism

Ruonan Bo[1,2,3†], Xiaopan Liu[1†], Jing Wang[1], Simin Wei[1], Xinyue Wu[4], Ya Tao[1], Shuya Xu[1], Mingjiang Liu[1,2,3], Jingui Li[1,2,3]* and Huan Pang[4]*

[1]College of Veterinary Medicine, Yangzhou University, Yangzhou, China, [2]Jiangsu Co-innovation Center for Prevention and Control of Important Animal Infectious Diseases and Zoonoses, Yangzhou, China, [3]Joint International Research Laboratory of Agriculture and Agri-Product Safety, The Ministry of Education of China, Yangzhou University, Yangzhou, China, [4]School of Chemistry and Chemical Engineering, Yangzhou University, Yangzhou, China

Atractylodes macrocephala Koidz (*A. macrocephala*) has been used both as a traditional medicine and functional food for hundreds of years in Asia. And it has a variety of biological activities, such as enhancing the ability of immunity and modulating effect on gastrointestinal motility. In this study, a water-soluble polysaccharide with molecular weight of 2.743×10^3 Da was isolated from the root of *A. macrocephala*. Polysaccharide from *A. macrocephala* (AMP) consisted of arabinose, galactose, glucose, xylose, mannose, ribose, galactose uronic acid, glucose uronic acid, with a percentage ratio of 21.86, 12.28, 34.19, 0.43, 0.92, 0.85, 28.79, and 0.67%, respectively. Zinc plays an important role in immune system. Therefore, we supposed that AMP binding with zinc oxide (ZnO) nanoparticles (AMP-ZnONPs) might be an effective immunostimulator. AMP-ZnONPs was prepared by Borch reduction, and its structural features were characterized by Scanning Electron Microscope (SEM), Transmission electron microscope (TEM), TEM-energy dispersive spectroscopy mapping (TEM-EDS mapping), Fourier transform infrared spectroscopy (FT-IR), X-ray photoelectron spectrometer (XPS), X-ray diffraction (XRD), particle size and zeta-potential distribution analysis. Then, its immunostimulatory activity and the underlying mechanism were evaluated using RAW264.7 cells. The results showed that AMP-ZnONPs remarkably promoted cell proliferation, enhanced phagocytosis, the release of nitric oxide (NO), cytokines (IL-6 and IL-1β) and the expression of co-stimulatory molecules (CD80, CD86 and MHCII). Moreover, AMP-ZnONPs could promote

the expression of Toll-like receptor 4 (TLR4), Myeloid differentiation factor 88 (MyD88), TNF receptor associated factor 6 (TRAF6), phospho-IκBα (P-IκBα) and phospho-p65 (P-p65), and TLR4 inhibitor (TAK242) inhibited the expression of these proteins induced by AMP-ZnONPs. Therefore, AMP-ZnONPs activated macrophages by TLR4/MyD88/NF-κB signaling pathway, indicating that AMP-ZnONPs could act as a potential immunostimulator in medicine and functional food.

KEYWORDS

polysaccharide from *Atractylodes macrocephala* Koidz, zinc oxide nanoparticles, immunostimulatory activity, TLR4 signaling pathways, potential immunostimulator

Introduction

In recent years, immunoregulatory polysaccharides are considered important macromolecules for stimulation of immune response, then gradually become a major research hot spot (1, 2). *Atractylodes macrocephala* Koidz *(A. macrocephala)* has been used both as traditional medicine and functional food for hundreds of years in Asia, and it was approved as a functional food by the National Health Commission of the People's Republic Health of China (3–5). Polysaccharide from *A. macrocephala* (AMP) has a variety of biological activities, such as enhancing the ability of immunity, modulating effect on gastrointestinal motility and decreasing the blood glucose level (6–8). However, a lot of natural polysaccharides exhibit only weak bioactivities due to the limitation of structural and conformational properties (9). Thus, further research about enhancing bioavailability of AMP is necessary.

Zinc (Zn) deficiencies in the body is a serious problem, which severely harms the health of the organism and causes the etiology of myocardial apoptosis, deregulated homeostasis (10–12). In addition, zinc is important for cellular homeostasis and also serves as a regulatory signaling molecule for immune cells (13, 14). Zinc oxide (ZnO) is listed as "commonly considered as safe" by the US Food and Drug Administration (FDA) (15). Some studies have shown that Zn has a significant role in the development and activation of effector cells of the innate and adaptive immune systems (16–18). ZnO nanoparticles (ZnONPs) have been exploited in biomedical and preclinical research for their advantages such as non-toxicity and low cost (19, 20). However, ZnONPs are limited their application in drug delivery due to their poor water solubility, strong agglomeration and less dispersion. Hence, it is imperative to develop an effective, safe and high-content Zn-supplement. To improve the dispersion of particles in water, a silane coupling agent (KH550) was used to modify the ZnONPs (21). In addition, KH550 was easily grafted at the ZnONPs interface, and the other side of KH550 carries an amino group that was easily grafted with polysaccharides.

Macrophages are one of the most important effector cells of the immune system, and play pivotal roles in the immune response (22). Phagocytosis is a marker of their activation. Upon activation, macrophages release NO, diverse cytokines and co-stimulatory molecules (23, 24). Many natural polysaccharides modulate the immune system through the activation of TLR4 in macrophages (25–29). Toll-like receptor 4 (TLR4), a key pattern recognition receptor involved in the activation of macrophages, is reported the major component of the signaling including nuclear factor-κB (NF-κB) signaling pathway.

We supposed that AMP binding with ZnONPs (AMP-ZnONPs) might provide a novel way to explore an effective immunostimulator. To enhance the dispersive capacity of ZnONPs in the water, γ-aminopropyltriethoxy silane (KH550) was applied to modify its surface. Then, AMP-ZnONPs was successfully prepared by the binding of KH550-ZnONPs and AMP *via* the Borch reduction between -NH_2 group and -CHO group (**Figure 1**). Its structural properties were characterized and then its immunostimulatory activities including cell viability, phagocytosis, surface molecules, cytokines release were evaluated using RAW264.7 cells. To further reveal the mechanism of immune stimulation, the effects of AMP-ZnONPs on the TLR4/MyD88/NF-κB signaling pathways were analyzed. This study is expected to provide new ideas for the development and utilization of polysaccharides and microelements in the food and pharmaceutical industry.

Materials and methods

Reagents and materials

A. macrocephala was purchased from the Tongrentang Company in Beijing. The plant material was identified by Prof. Jingui Li. The purified AMP was prepared in our laboratory and the polysaccharide content was 96% (UV). RAW264.7 cells were obtained from American Type Culture Collection (ATCC,

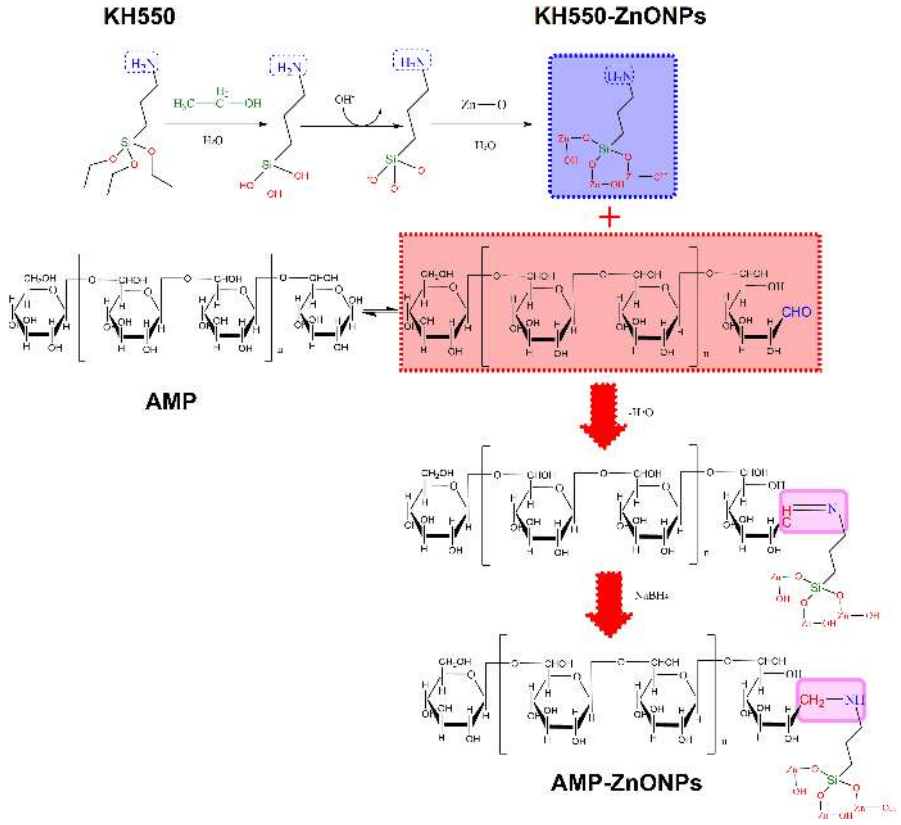

FIGURE 1
Schematic illustration of AMP-ZnONPs synthesis. The surface of ZnONPs was modified with KH550 through Borch reduction and then AMP was bond to the KH550-ZnONPs.

Rockville, MD, United States). Fucose (Cat No. B25632), arabinose (Cat No. B65342), rhamnose (Cat No. B50770), galactose (Cat No. B21893), glucose (Cat No. B21882), xylose (Cat No. B21880), mannose (Cat No. B21895), fructose (Cat No. B21896), ribose (Cat No. B21897), galacturonic acid (Cat No. B21894) and glucuronic acid (Cat No. B25302) were purchased from Shanghai Ye Yuan Biotechnology Co., Ltd. FITC-dextran (Cat No. 60842-46-8) and fetal bovine serum (Cat No. F8318) were purchased from Sigma Corporation of America. DMEM culture solution (Cat No. SH30022.01) was purchased from HyClone. NO test kit (Cat No. S0021) was obtained from Beyotime Biotechnology. Silane coupling agent (KH550, Cat No. A7440) and ZnONPs (purity 99.9%, Cas No. 1314-13-2) were the products of Sinopharm Chemical Reagent Ltd. RNA-easy Isolation Reagent (Cat No. R701) was purchased from Vazyme Biotech Co., Ltd. The CCK8 (Cat No. 40203ES80), Hifair® III 1st Strand cDNA Synthesis SuperMix for qPCR (gDNA digester plus) (Cat No. 11141ES60) and Hieff® qPCR SYBR Green Master Mix (High Rox Plus) (Cat No. 11184ES08) were the products of Yeasen Biotech Co., Ltd. Rabbit Anti-CD80 Polyclonal Antibody (Cat No. bs-1479R), Rabbit Anti-CD86 Polyclonal Antibody (Cat No. bs-1035R) and Rabbit Anti-MHC Class II/HLA DMB Polyclonal Antibody (Cat No. bs-4107R) were purchased from Biosynthesis Biotechnology Inc. (Beijing, China). Antibodies of TLR4 (Cat No. 14358s), TRAF6 (Cat No. 67591s), MyD88 (Cat No. 4283s), phospho-IκBα (P-IκBα) (Cat No. 4812s), phospho-p65 (P-p65) (Cat No. 8242s) and β-actin (Cat No. 4970s) were the products of Cell Signaling Technology Pathways. TLR4 inhibitor (TAK242, Cat No. M4838) was purchased from Abmole (Houston, TX, United States).

Extraction and purification of polysaccharide from *Atractylodes macrocephala*

AMP was extracted by water extraction and alcohol precipitation methods. Briefly, *A. macrocephala* was first extracted with alcohol for 2 times to remove the impurity. Second, *A. macrocephala* was decocted in water. The aqueous extract was concentrated under a vacuum. After that, a threefold volume of alcohol was added, the precipitated was washed three times with anhydrous ethanol, acetone and diethyl

(30). Then, the protein was removed using sevage methods (31). The polysaccharide was dialyzed for 24 h. We further purified the crude polysaccharide through Sephadex G-100 column. Finally, the purified extraction was lyophilized and the polysaccharide content of AMP was determined by UV-VIS absorption spectrometry.

Molecular weight measurement of polysaccharide from *Atractylodes macrocephala*

The molecular weight of purified samples was determined by high-performance gel permeation chromatography (HPGPC; Agilent 1,260 Infinity). Three gel permeation columns (KS-805, KS-804 and KS-802) were linked in serials. The column temperature was kept at 70°C. Double distilled water was used as mobile phase and the flow rate was kept at 1 mL·min^{-1}. The calibration curve was constructed using different molecular weights of Dextran standards, and the molecular weight of AMP was calculated by Dextran standards.

Monosaccharide composition analysis of polysaccharide from *Atractylodes macrocephala*

5 mg of AMP and 1 mL of trifluoroacetic acid (TFA, 2 M) were hydrolyzed at 121°C for 2 h. The mixture was dried with nitrogen, and then washed with methanol 2–3 times followed. The monosaccharide standards included fucose, arabinose, rhamnose, galactose, glucose, xylose, mannose, fructose, ribose, galacturonic acid and glucuronic acid. Finally, samples were analyzed *via* high-performance anion-exchange chromatography (HPAEC) (ICS5000, Thermo Fisher Scientific, United States) with Dionex^{TM} CarboPac^{TM} PA-20 column (150 mm × 3.0 mm, 10 μm). Mobile phase A was 0.1 M NaOH, mobile phase B was 0.1 M NaOH, 0.2 M NaAc. The composition of eluent A was adjusted to 95% at 0 min, 80% at 30 min, 60% at 30.1 min, 60% at 45 min, 95% at 45.1 min, 95% at 60 min. The column temperature was 30°C. The flow rate was 0.5 mL·min^{-1} and the injection volume was 5 μL. The determination of monosaccharide composition was made with an electrochemical detector and the peaks were processed using Chromeleon 7.2 CDS (Thermo Scientific).

Preparation of AMP-ZnONPs

In order to fully hydrolyze KH550, 4 mL KH550 was added to 400 mL of equal volumes of alcohol and water, the mixture was reacted for 10 min under ultrasonication, and then agitated for 20 min on a magnetic stirrer. The pH of the solution was adjusted to between 6.5 and 7.0 with 0.2 M HCl to generate silicon-oxygen bonds for grafting the ZnONPs. Then, 4.5 g of ZnONPs was added to this solution, sonicated for 30 min, agitated for 30 min at 200 rpm on a magnetic stirrer (80°C), and then the mixture was collected and lyophilized. The surface of ZnONPs was modified with KH550 by these processes. KH550-ZnONPs (10 mg) was added to water (20 mL). After sonicating for 1 h, AMP was added to the KH550-ZnONPs (m_{AMP}: $m_{KH550-ZnONPs}$ = 4:1) and stirred for 24 h. The -CHO of AMP and the -NH_2 of ZnONPs were linked to assemble AMP-ZnONPs by Borch reduction.

Characterization of AMP-ZnONPs

Scanning Electron Microscope (SEM, Zeiss Supra55, Germany) was used to detect the samples of ZnONPs, KH550-ZnONPs, AMP and AMP-ZnONPs, the image magnification was 5,000 x. The morphology of samples was also observed *via* a Transmission electron microscope (TEM, HT7800, Hitachi, Japan). The element distribution was observed by Transmission electron microscope-energy dispersive spectroscopy mapping (TEM-EDS mapping, Tecnai G2 F30 S-TWIN, FEI, US) to verify the connection of the ZnONPs and AMP. The Fourier transform infrared spectroscopy (FT-IR, Thermo Electron Corporation, United States) spectra were recorded in the mid-infrared region. The samples were determined at room temperature on an X-ray diffraction (XRD, D8 Advance, Germany), and operated at 40 kV and 40 mA. The samples were determined with X-ray photoelectron spectrometer (XPS, ESCALAB 250Xi, United States). Data were analyzed using the Avantage software. The laser particle size analyzer (NanoPlus 3, Micromeritics Instrument Corp., United States) was applied to measure average particle size, polydispersity index (PDI) and zeta-potential.

Cell culture

RAW264.7 cells were cultured in the Dulbecco's modified Eagle's medium (DMEM) with 10% fetal bovine serum. Cells were maintained under a humified atmosphere at 37°C with 5% CO_2.

Cell activity assay

The cell activity of AMP and AMP-ZnONPs on RAW264.7 cells was determined according to the CCK-8 method. Cell viability of RAW264.7 cells was evaluated after treatment with AMP and AMP-ZnONPs (0.06–250 μg·mL^{-1}) for 24 h. Following this, the supernatants were discarded, then added fresh DMEM medium (100 μL·well^{-1}) containing CCK8 (10

$\mu L \cdot well^{-1}$) and cultivated for 1.5–4 h at 37°C. Finally, the absorbance at 450 nm was measured by microplate reader. The cell survival rate was calculated as follows:

$$\text{Cell activity (\%)} = A_2/A_1 \times 100\%$$

(Where A_1 and A_2 are the absorbances of the control and test samples, respectively).

Measurement of nitric oxide

In brief, RAW264.7 cells (1×10^5 cells$\cdot mL^{-1}$) were separately exposed to ZnONPs, AMP-ZnONPs and AMP (1.95 $\mu g \cdot mL^{-1}$) for 24 h at 37°C in a constant temperature incubator ventilating with 5% CO_2. At the end of incubation, the NO amount in the supernatant was measured by a Griess reagent system kit K.

Quantitative real-time polymerase chain reaction

Real-time polymerase chain reaction (PCR) was employed for the determination of cytokines (IL-6 and IL-1β) and TLR4, MyD88, TRAF6 mRNA expression. The total RNA of RAW264.7 cells was obtained with Trizol reagent, and then synthesized the corresponding cDNA. The Hieff qPCR SYBR Green Master Mix was employed to perform Quantitative real-time PCR assay. The primer sequences of genes were displayed in **Table 1**. The following PCR protocol was referenced by our previous report (32). The expression of each gene was analyzed by the $2^{-\Delta\Delta ct}$ comparative method.

Determination of phagocytic function using CytExpert flow cytometer

RAW264.7 cells ($1 \times 10^6 \cdot mL^{-1}$) were cultured in 6 well plates at 37°C for 12 h, and then exposed to ZnONPs, AMP, AMP-ZnONPs (1.95 $\mu g \cdot mL^{-1}$) or LPS (0.5 $\mu g \cdot mL^{-1}$) for 24 h, respectively. The cells were incubated with 1 $mg \cdot mL^{-1}$ FITC-dextran for 1 h, then the reaction was stopped by cold PBS. The FITC-dextran intensity of cell samples was analyzed by CytExpert flow cytometer (Beckman Coulter, CA, United States).

High-resolution laser confocal microscopy

Cells were seeded at 1×10^5 cells$\cdot mL^{-1}$ on coverslips in a 24 well plate, then stimulated with ZnONPs, AMP, AMP-ZnONPs (1.95 $\mu g \cdot mL^{-1}$) or LPS (0.5 $\mu g \cdot mL^{-1}$), and incubated with 1 $mg \cdot mL^{-1}$ FITC-dextran (1 $mg \cdot mL^{-1}$) at 37°C for 1 h. After incubation, RAW264.7 cells were fixed with 4% paraformaldehyde for 10 min. Cell samples were stained with phalloidin for 1 h under dim light, followed by DAPI staining. The green fluorescence was measured by laser confocal microscopy (LSCM) (TCS SP8 STED, Germany).

Expression of cell surface molecule CD80, CD86, and MHCII

The cells (1×10^6 cells$\cdot mL^{-1}$) were treated with AMP-ZnONPs for 24 h in a 6-well plate. Then, the cells were suspended and incubated with anti-CD80, anti-CD86 and anti-MHCII at 4°C for 30 min, and analyzed by the CytExpert flow cytometer.

Cell morphological observation

The cells (1×10^5 cells$\cdot mL^{-1}$) were plated on coverslips in 24-well plates, and then treated with ZnONPs, AMP, AMP-ZnONPs (1.95 $\mu g \cdot mL^{-1}$), LPS (0.5 $\mu g \cdot mL^{-1}$) or DMEM. The RAW264.7 cells with glutaraldehyde-treated were prepared for 24 h. Next, the cells were evaporated using a 30, 50, 70, 80, 90, 95, and 100% ethanol gradient (10–15 min each time); then displaced in Na_2SO_4, dried at a tipping point, and finally scanned by SEM (HT7800, Hitachi, Japan) at 1,000 and 8,000×.

Western blotting analysis

The BCA protein assay kit was employed to detect the protein concentrations. Equal amounts (30 μg) of total protein were separated and transferred to the NC membrane (33). The membrane was incubated with 5% skim milk for 2 h and then incubated with gentle shaking with primary antibodies at 4°C overnight. Later incubated NC at 4°C with antibodies of TLR4 (rabbit, 1: 1,000), TRAF6 (rabbit, 1: 1,000), MyD88 (rabbit, 1: 1,000), P-p65 (rabbit, 1: 1,000), P-IκBα (rabbit, 1: 1,000) and ß-actin (rabbit, 1: 1,000). After incubation with the primary antibody, the membrane was exposed to goat anti-rabbit secondary antibody (1: 5,000) at room temperature for 1 h. The membrane was washed with TBST for 3 times, membrane-bound antibodies were visualized using the ECL Enhanced Chemiluminescence system, the protein band intensity was analyzed with Image J Analysis Software.

Statistical analysis

GraphPad Prism 5.0 Software was utilized for statistical analysis. Data were analyzed by one-way analysis of variance

(ANOVA) followed by Dunnett's multiple comparisons test. All the data were expressed using mean ± standard deviation (SD). The criterion of significance was $P < 0.05$.

Results and discussion

Molecular weight and monosaccharide composition of polysaccharide from *Atractylodes macrocephala*

As shown in Figure 2A, the results of HPGPC implied a good homogeneity of AMP. The retention time was 24.98 min. The chromatographic result of HPGPC showed that AMP had one peak, which indicated that AMP was homogeneous polysaccharides. Based on the regression equation of the dextran standard curve, y = 11.864079–0.338831×–0.005080×^2 + 0.000195×^3, the molecule weight of AMP was calculated as 2.743×10^3 Da (Figure 2B). The result of monosaccharide composition obtained from AMP was described by HPAEC (Figures 2C,D). AMP was composed of arabinose, galactose, glucose, xylose, mannose, ribose, galactose uronic acid, glucose uronic acid, with a percentage ratio of 21.86, 12.28, 34.19, 0.43, 0.92, 0.85, 28.79, and 0.67%, respectively.

Characteristics of AMP-ZnONPs

Morphological characteristics of AMP-ZnONPs

Untrastructure of ZnONPs, KH550-ZnONPs, AMP and AMP-ZnONPs was obtained with the SEM (Figure 3A). The AMP exhibited an irregular surface with many folds. ZnONPs showed rod morphology and a nano-lamellar structure. The KH550-ZnONPs after the surface modification displayed particles with uniform size, good monodispersity, and no obvious agglomeration. The surface of AMP appeared to be covered by rod-shaped ZnONPs, which was attributed to the strong interaction between amino in ZnONPs and hemiacetal in AMP because of hydroamination. Ultrastructure of ZnONPs, KH550-ZnONPs, AMP and AMP-ZnONPs as shown in Figure 3B. The ZnONPs showed strong clustering and exhibited aggregation. The KH550-ZnONPs had smaller clusters and showed a homogenous dispersion, all aggregation was disrupted. As shown in the AMP-ZnONPs, KH550-ZnONPs were connected to the surface of AMP. The TEM-EDS mapping and EDS spectra showed that C, O and Zn elements were present in AMP-ZnONPs (Figure 3C). Therefore, the results strongly supported the formation of AMP-ZnONPs.

Fourier transform infrared spectroscopy analysis

As shown in Figure 4A, FT-IR spectra of AMP revealed that the characteristic peaks of polysaccharide at 3366.9 cm^{-1}, 2931.4 cm^{-1}, and 1427 cm^{-1} were attributed to O-H stretch vibration of hydroxyl group, C-H stretch vibration and O-H bending vibration, respectively (34). Moreover, the weak bands around 935.6 cm^{-1} and 818.9 cm^{-1} indicated that there were α-configuration and β-configuration (35, 36). FT-IR spectra of ZnONPs showed an intense peak at 571.1 cm^{-1} and a broad peak at 3442.1 cm^{-1}. The weak absorption peak at 3442.1 cm^{-1} could be attributed to stretching vibration of associating hydroxyls formed by weak hydrogen bonding as well as van der Waals interaction (37). The stretching vibration band at 571.1 cm^{-1} corresponding to the Zn-O bond (38). Compared with ZnONPs, KH550-ZnONPs displayed a new typical characteristic absorption peak of -NH_2 at 1582.6 cm^{-1}, which was attributed to the characteristic absorption peak of KH550. The AMP-ZnONPs spectra showed the characteristic absorption peaks of ZnONPs, KH550 and AMP. In addition, the signal in 1058.9 cm^{-1} was mainly assigned to the stretching vibration of the C-O-C group, the absorption peak at 1,629 cm^{-1} corresponded to N-H stretching vibrations (39, 40). FT-IR spectra of AMP showed that the band at 1636.2 cm^{-1} corresponding to the C = O bond (41). There was no N-H bond in AMP, after connecting to ZnONPs, the presence of an N-H bond in AMP-ZnONPs indicated a possible connection. The result provided evidence for the successful grafting of the KH550-ZnONPs by the NH_2 groupings in KH550 agents onto AMP.

X-ray diffraction analysis

XRD, as a valuable instrument (42), could be used to further confirm the composition of AMP-ZnONPs (Figure 4B). The

TABLE 1 The primer sequences of target genes.

Gene	Sense (5′–3′)	Antisense (5′-3′)
IL-6	TTCCATCCAGTTGCCTTCTTG	AATTAAGCCTCCGACTTGTGAA
IL-1β	ATCTCGCAGCAGCACATCA	CCAGCAGGTTATCATCATCATCC
TLR4	TGGTCAGTGTGATTGTGGTATC	GCTTTCTCCTCTGCTGTACTT
MyD88	TCGATGCCTTTATCTGCTACTG	GGTCGGACACACACAACTTA
TRAF6	GCTGAGCCACAATACTCACTAA	TTCTAGCGGATGGACATTACAC
GADPH	ATGGTGAAGGTCGGTGTGAA	CCTTGACTGTGCCGTTGAAT

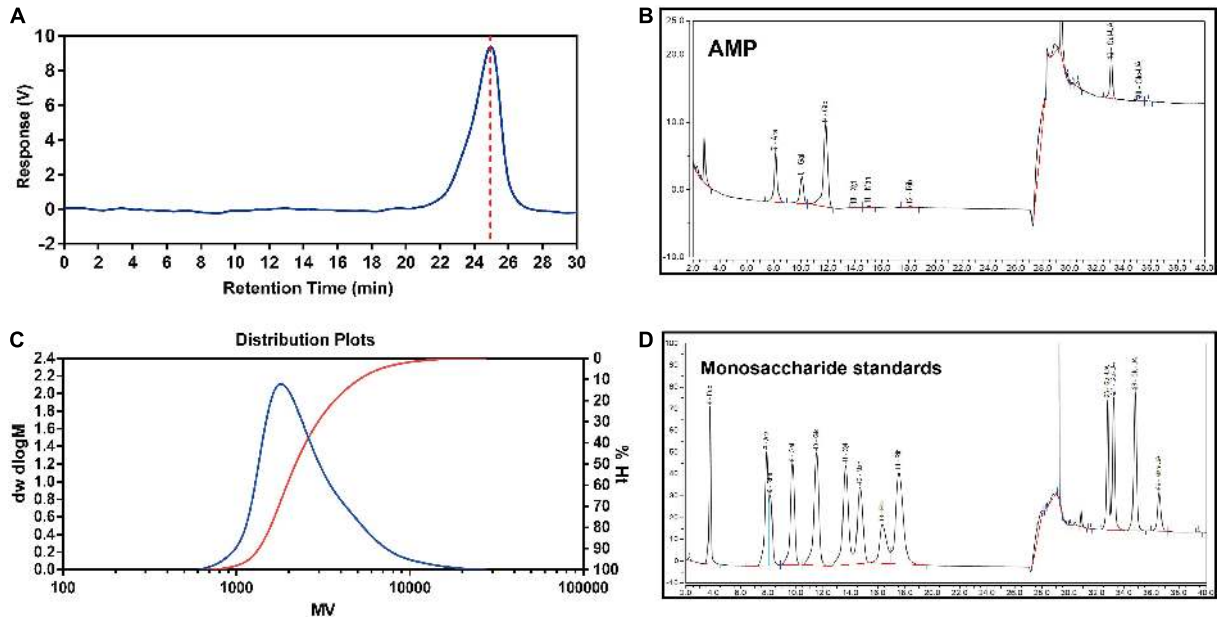

FIGURE 2
Molecular weight and monosaccharide composition of AMP. The peak at retention time of AMP **(A)** and molecular weight distribution **(B)** of AMP. HPAEC chromatograms of AMP **(C)** and monosaccharide standards **(D)**. Fuc, fucose; Ara, arabinose; Rha, rhamnose; Gal, galactose; Glc, glucose; Xyl, xylose; Man, mannose; Fru, fructose; Rib, ribose; Gal-UA, galacturonic acid; Glu-UA, glucuronic acid.

characteristic peaks located at 2θ = 31.7, 34.4, 36.2, 47.5, 56.6, 62.8, 66.3, 67.9, 69.1, 72.5, 76.9, corresponding to the (100), (002), (101), (102), (110), (103), (200), (112), (201), (004), (202) planes, respectively, match well with characteristic reflections of ZnONPs (P63mc, JCPDS no. 89-0511). A similar curve of ZnONPs modified by KH550 proved that modification of KH550 did no effect on the phase formation of ZnONPs. The XRD results of AMP recorded between 10° and 30° suggested the presence of crystalline components, with major reflections at 12.0°, 17.7° and 21.8°. This profile was also observed in other different polysaccharides (43, 44). The XRD profile of AMP-ZnONPs showed that the main characteristic peaks of ZnONPs, confirming that the hexagonal structure of the ZnONPs was not affected after binding with AMP. Moreover, as sreov-shapederot affected aft θ = 10–20, the modified AMP molecule maybe undergo a chemical structure change and convert to amorphous materials under this circumstance.

X-ray photoelectron spectrometer analysis

XPS was depicted in **Figure 4C** to investigate the surface compositions of the ZnONPs (45, 46). Compared with ZnONPs, the XPS spectra of the KH550-ZnONPs exhibited the characteristic peak components of Zn2p3, O1s, N1s, C1s and Si2p, suggesting that silane had successfully modified on the surface of ZnONPs. The AMP showed a Zn-free surface, the two peaks at 285, and 532 eV correspond to C1s and O1s, respectively. The C1s core-level spectrum of the KH550-ZnONPs was divided into three peak components: C-C, C-N and C-Si (**Figure 4D**). The C1s core-level spectrum of the AMP was divided into two peak components: C-C and C-O (**Figure 4E**). The peaks of C-O (286.6 eV), C-C (284.8 eV), C-N (286.3 eV) and C-Si (283.5 eV) were also observed in the C1s spectrum of the AMP-ZnONPs (**Figure 4F**), the C-N single bond peak was introduced by KH550, and the C-O peak was introduced by AMP. The presence of a C-N bond confirmed that there was a cross-linking reaction between the AMP and the KH550-ZnONPs. Although the Zn2p3 peak was reduced due to the AMP shielding, some active sites of ZnONPs remain even. These results were in good agreement with previous results of XRD and FT-IR, indicating that the successful grafting of AMP and KH550-ZnONPs.

Particle size, polydispersity index and zeta potential

The particle size (**Table 2** and **Figure 5A**) of the ZnONPs was larger than that of the KH550-ZnONPs, this result revealed that after KH550 being modified on the surface of ZnONPs promoted the particle size to be smaller. The particle size of AMP-ZnONPs was slightly larger than KH550-ZnONPs, which may be caused by the AMP binding on KH550-ZnONPs. The PDI values of AMP-ZnONPs was lower than 0.3, which was considered optimal for the dispersion and homogeneity (47). The zeta potential of AMP-ZnONPs was more negatively charged than KH550-ZnONPs (**Figure 5B**), with AMP-ZnONPs gaining additional negative charge of −4.43 mV. Negatively

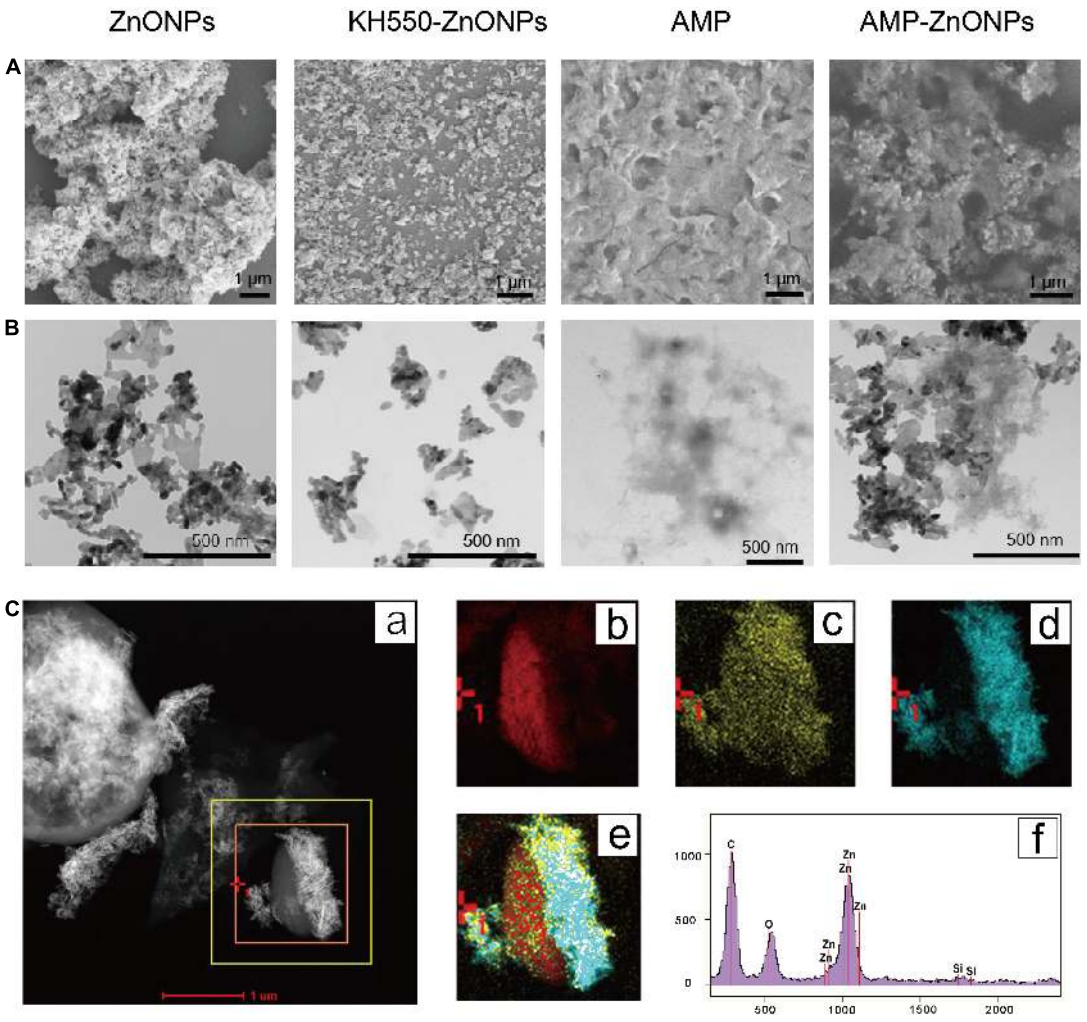

FIGURE 3
The SEM analyzes of ZnONPs, KH550-ZnONPs, AMP and AMP-ZnONPs **(A)**. The TEM analyzes of ZnONPs, KH550-ZnONPs, AMP and AMP-ZnONPs **(B)**. TEM-EDS mapping image of AMP-ZnONPs **(C)**, TEM image (a), corresponding elements distribution of C (b), O (c) and Zn (d), merge (e), EDS spectrum (f).

charged nanoparticles are more likely to be internalized by cells than positively charged nanoparticles, this property underlies the fact that AMP-ZnONPs stimulates phagocytosis of RAW264.7 cells more significantly than either ZnONPs or AMP alone.

Cell viability

The cell viability of ZnONPs, AMP and AMP-ZnONPs on RAW264.7 cells were shown in Figure 6A. Compared with the control group, ZnONPs, AMP and AMP-ZnONPs exerted no damaging effect and promoted cell proliferation to a certain extent at a concentration of 0.24–1.95 $\mu g \cdot mL^{-1}$. When the concentration of AMP-ZnONPs was 0.49–3.91 $\mu g \cdot mL^{-1}$, the proliferation effect was proportional to the concentration. To compare the immune effects of ZnONPs, AMP and AMP-ZnONPs at the same concentration level, the concentration of ZnONPs, AMP and AMP-ZnONPs at 1.95 $\mu g \cdot mL^{-1}$ were chosen in the following experiments.

AMP-ZnONPs induced cells nitric oxide production

NO is an important active substance associated with the immunomodulatory effect (48), which participates in apoptosis regulation and host defense function (49). The NO production was calculated from the standard curve formula. The results of NO release in AMP-ZnONPs were shown in Figure 6B. As a positive control, the NO content of LPS group (0.5 μgPS^{-1}) showed significantly higher than the control group ($P < 0.001$). And the release of NO in AMP-ZnONPs group was higher than that of the control, ZnONPs group ($P < 0.001$) and AMP group ($P < 0.05$). Therefore, AMP-ZnONPs could stimulate NO

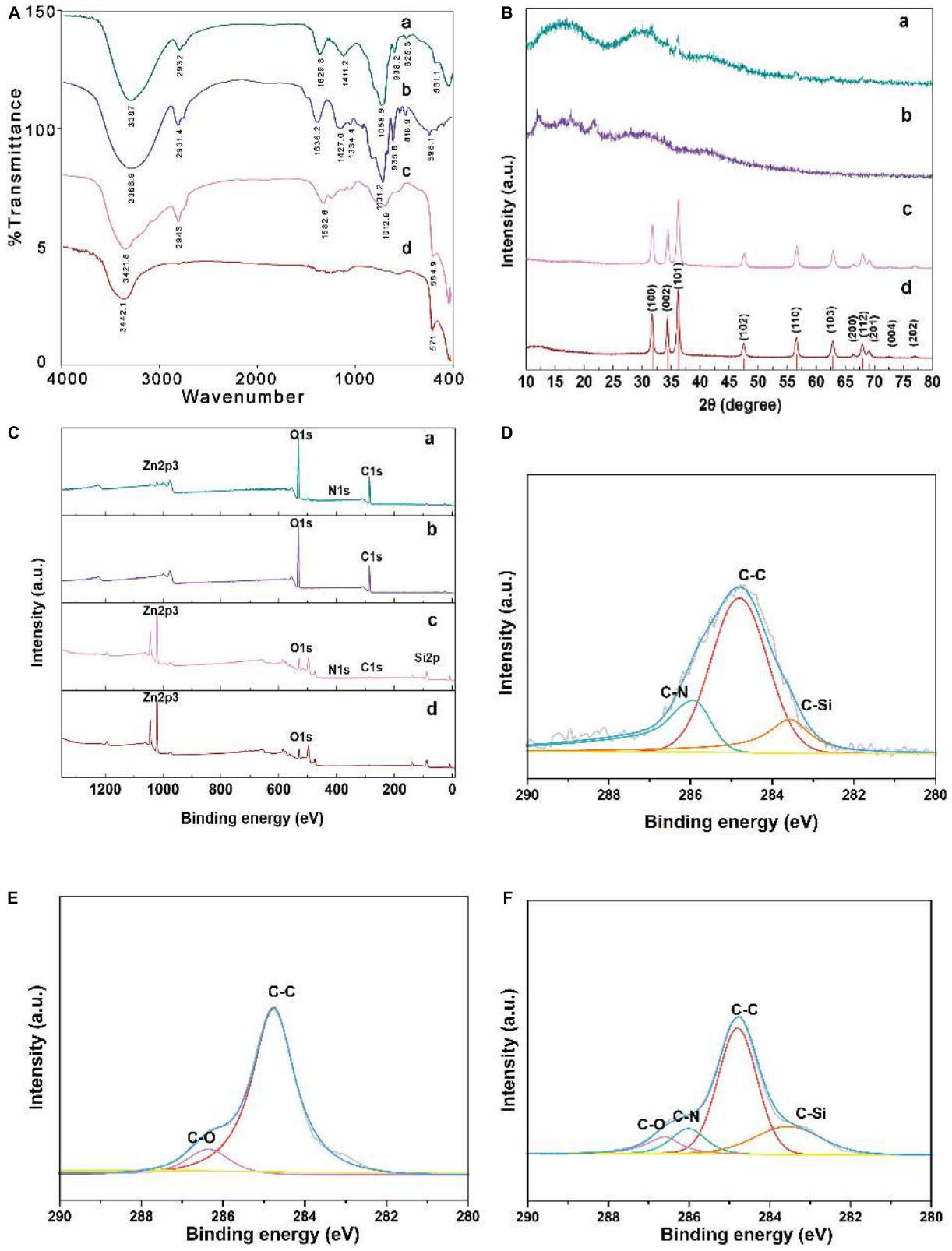

FIGURE 4
Spectroscopic characterization and curve-fitting spectra of AMP-ZnONPs. The FT-IR pattern **(A)**, XRD pattern **(B)**, XPS spectra **(C)** of AMP-ZnONPs (a), AMP (b), KH550-ZnONPs (c) and ZnONPs (d). The curve-fitting of C1s **(D)** spectra of KH550-ZnONPs. The curve-fitting of C1s **(E)** spectra of AMP. The curve-fitting of C1s **(F)** spectra of AMP-ZnONPs.

TABLE 2 The particle size, PDI, and zeta potential of ZnONPs, KH550-ZnONPs and AMP-ZnONPs (n = 3).

Samples	ZnONPs	KH550-ZnONPs	AMP-ZnONPs
Size (nm)	211.89 ± 8.98	136.73 ± 3.12	391.37 ± 3.27
PDI	0.095 ± 0.053	0.391 ± 0.137	0.206 ± 0.086
Zeta potential (mV)	−33.20 ± 1.11	−10.97 ± 0.32	−15.40 ± 0.35

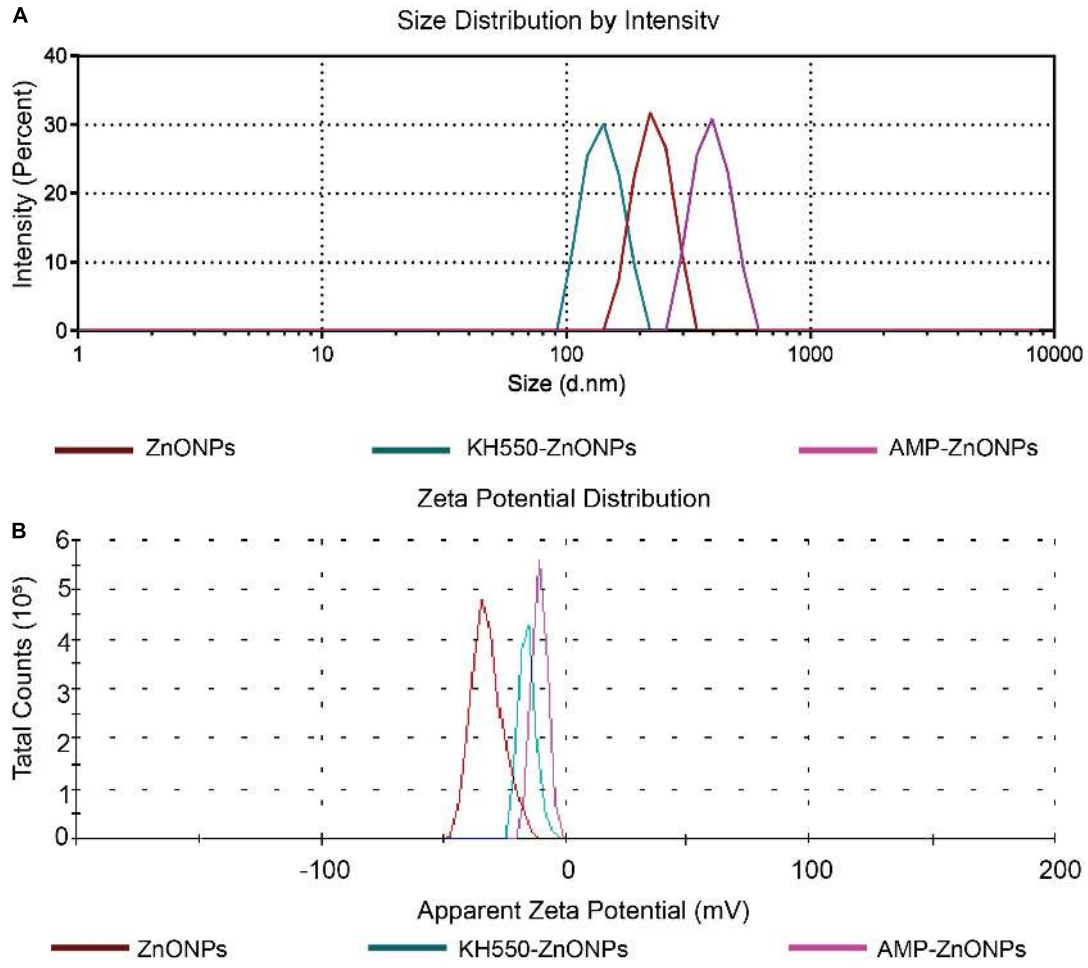

FIGURE 5
The particle size **(A)** and Zeta potential **(B)** of ZnONPs, KH550-ZnONPs and AMP-ZnONPs.

release more than AMP and ZnONPs in RAW264.7 cells, this suggested that ZnONPs displayed synergy with AMP.

AMP-ZnONPs induced cells cytokines secretion

Cytokines are the central logical targets for immune modulation as they influence the formation of a phenotype. They act as immunoregulators by either inducing or suppressing the production and maturation of immune cells (50). IL-1β is a major mediator of inflammation secreted by various activated innate immune cells, such as macrophages, monocytes and dendritic cells (51). IL-6 is also one of the important mediators that can stimulate antibody production and participate in immune response. Both IL-1β and IL-6 are of great importance for immune homeostasis and barrier immunity. To further investigate the immunological activity of AMP-ZnONPs on RAW264.7 cells, the cytokine (IL-1β and IL-6) contents in cells were evaluated by RT-qPCR in this study (**Figures 6C,D**). LPS stimulated the production of IL-1β and IL-6 by more than 2,000 times compared to the control group ($P < 0.001$), which indicated that LPS could promote inflammation and lead to excessive cytokine release (52). Notably, AMP-ZnONPs treatment exerted a significant action on IL-1β and IL-6 secretion than both AMP and ZnONPs ($P < 0.001$), which showed ZnONPs exerted a synergistic effect with

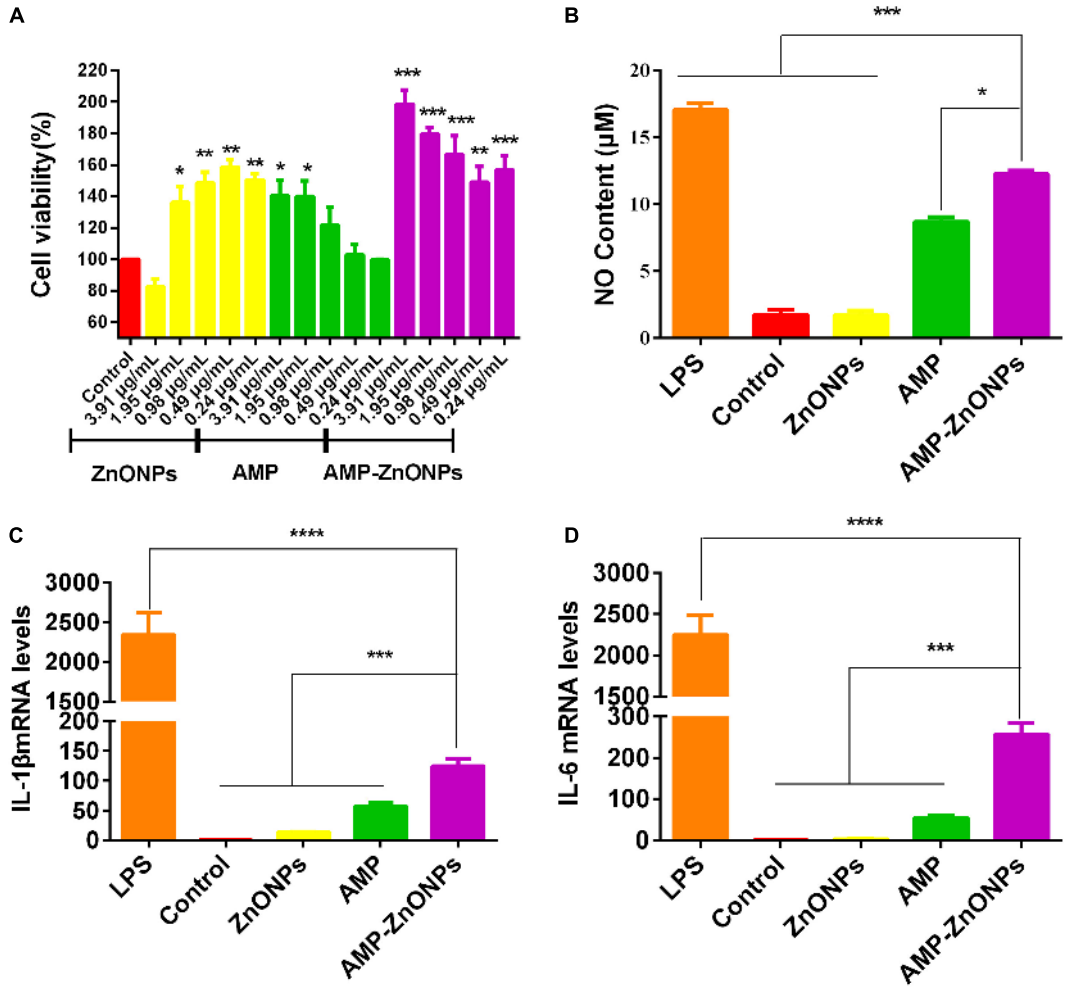

FIGURE 6
The proliferative activity of RAW264.7 cells stimulated by ZnONPs, AMP and AMP-ZnONPs **(A)**. NO content of cell culture supernatant **(B)** and the mRNA expression of IL-1β **(C)**, IL-6 **(D)** in RAW264.7 cells of different groups. (*$P < 0.05$, **$P < 0.01$, ***$P < 0.001$, ****$P < 0.0001$ vs. AMP-ZnONPs).

AMP. The results indicated that the AMP-ZnONPs had immunostimulatory effect, but it did not cause cell inflammation like LPS.

AMP-ZnONPs enhanced cells phagocytosis

Macrophages exist in virtually all tissues, phagocytosis, which is a classic index to evaluate macrophage activation, plays a critical role in the uptake and degradation (53–55). In addition, it is a signal-inducing process in which phagosomes bind to the antibody on the cell surface, consequently, cell morphology and signaling pathways are affected (56). The enhanced phagocytosis is one of the remarkable characteristics of activated macrophages, meanwhile indicating the activation of innate immunity. The results showed that compared with the control and ZnONPs, AMP-ZnONPs and AMP could significantly promote cell phagocytosis of macrophages (**Figures 7A,B**). Meanwhile, it should be highlighted that the stimulating effect of AMP-ZnONPs on phagocytosis was remarkably higher than AMP ($P < 0.05$). Furthermore, FITC-dextran accumulation in RAW264.7 was measured by LSCM. As shown in **Figure 7C**, AMP-ZnONPs treatment markedly enhanced the fluorescence intensity of tested cells relative to AMP and ZnONPs, and the FITC-dextran were mainly distributed in the cytoplasm. These results demonstrated that the AMP binding with ZnONPs significantly improved the immune activity of RAW264.7, which indicated ZnONPs and AMP acted in synergy of immune system.

AMP-ZnONPs promoted cells costimulatory molecules expression

The activation and further differentiation of T cells and cellular immune function are closely related to the function of antigen-presenting cells (APC), especially macrophages, considered as professional antigen-presenting cells (57). CD80

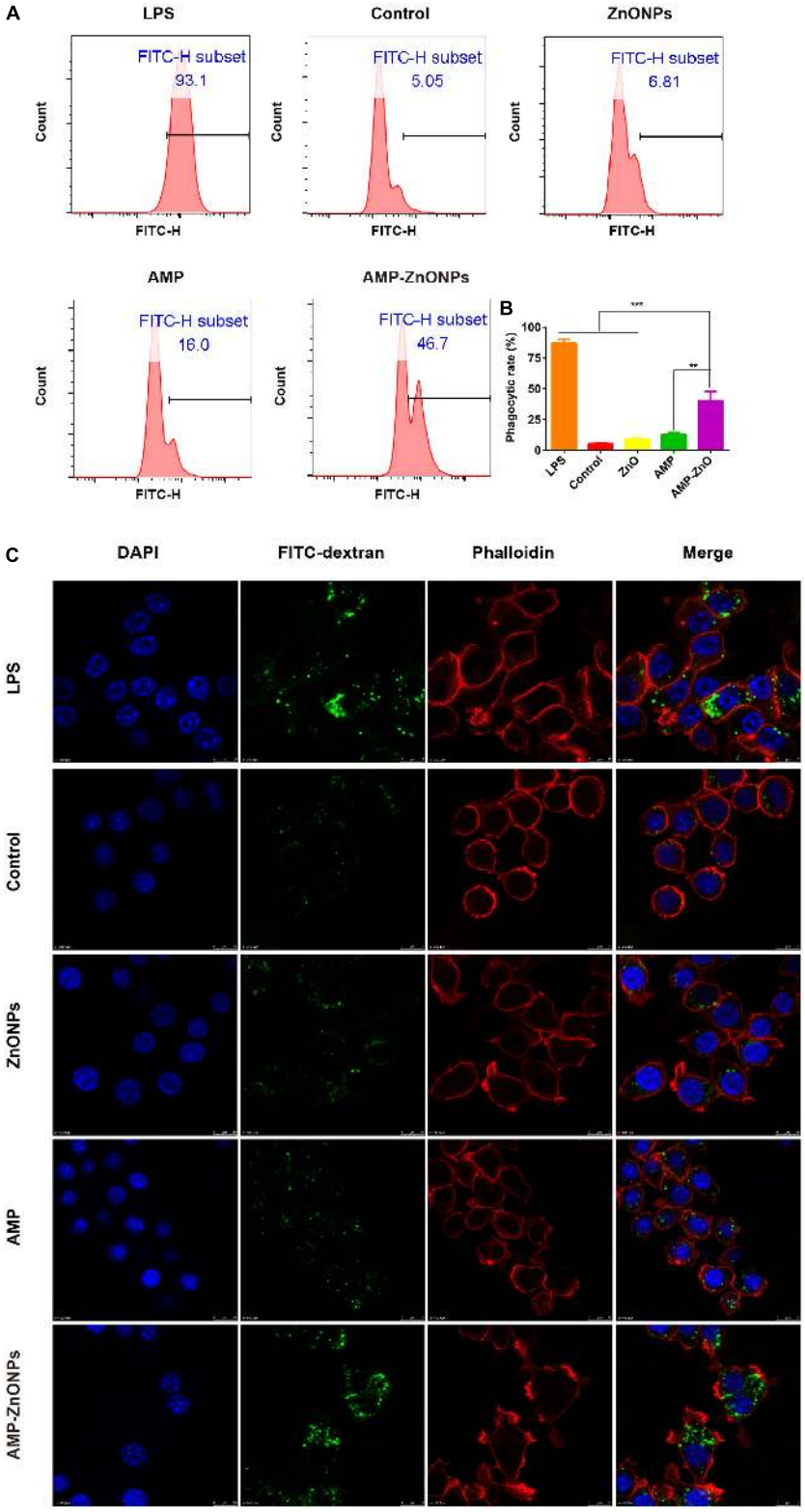

FIGURE 7
The phagocytosis was evaluated by flow cytometry **(A)**. The histogram showed the positive rate of cells for FITC-dextran **(B)**. (**$P < 0.01$, ***$P < 0.001$ vs. AMP-ZnONPs). Enhanced FITC-dextran uptake into RAW264.7 cells following incubation with AMP-ZnONPs. FITC-dextran (green) was mixed with ZnONPs, AMP, AMP-ZnONPs, LPS and DMEM medium (control) overnight avoiding light. Cytoskeleton and cell nuclei were stained with phalloidin (red) and DAPI (blue) respectively, **(C)**.

and CD86 may differentially control the T-cell activation because of the distinct properties of each molecule. Once presented to T cells by MHCII, peptide antigens generally stimulate a typical T cell-dependent immune response and the induction of immune memory (58). In this study, the expression of phenotypic markers of CD80, CD86 and MHCII up-regulated after the RAW264.7 cells were exposed to LPS for 24 h (Figure 8A). Figures 8B–D documented a significant increase in the percent of RAW264.7 cells positive for the expression of CD80, CD86, and MHCII following incubation with AMP-ZnONPs as compared to the control, ZnONPs and AMP. The results proved that AMP-ZnONPs significantly increased the expression of CD80, CD86 and MHCII compared with ZnONPs or AMP alone, which indicated ZnONPs and AMP showed synergetic effect with each other.

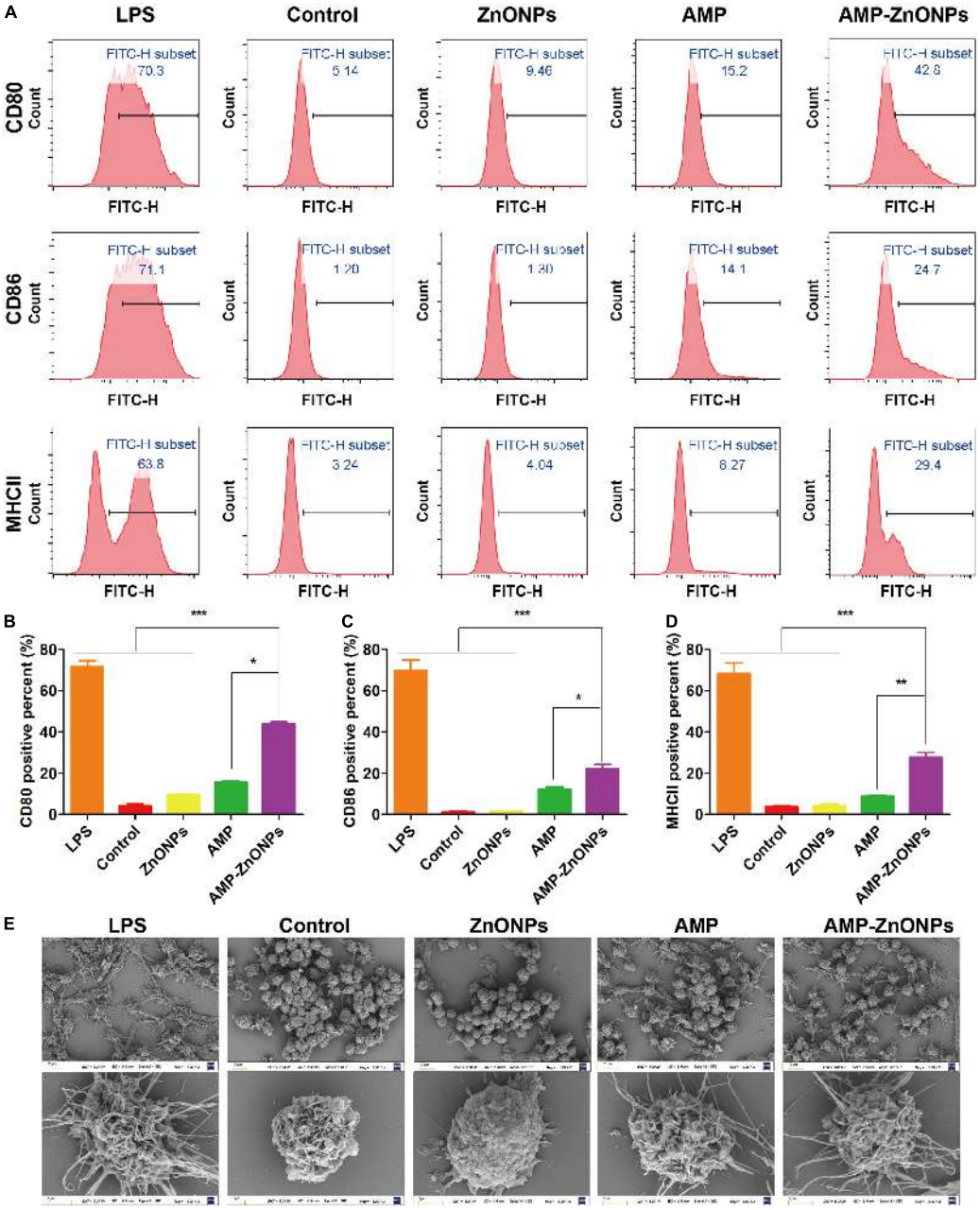

FIGURE 8
The production of CD80, CD86, MHCII in RAW264.7 cells were analyzed by flow cytometry **(A)**. The histogram showed the positive rate of CD80 **(B)**, CD86 **(C)**, MHCII **(D)** in cells. (*$P < 0.05$, **$P < 0.01$, ***$P < 0.001$ vs. AMP-ZnONPs). SEM analysis for morphological changes of RAW264.7 cells in different groups **(E)**.

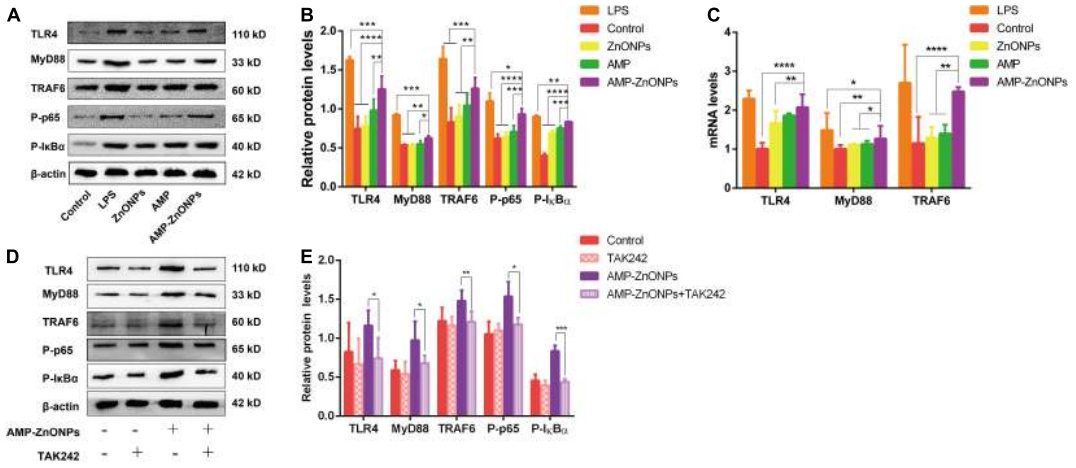

FIGURE 9
The relative expressions of proteins **(A,B)** and mRNAs **(C)** of the critical nodes in the TLR4/MyD88/NF-κB signaling pathways. Effects of TAK242 on TLR4, MyD88, TRAF6, P-IκBα and P-p65 expression stimulated by AMP-ZnONPs or not **(D,E)**. The results were expressed as the mean ± SD (n = 3) (*P < 0.05, **P < 0.01, ***P < 0.001, ****P < 0.0001 vs. AMP-ZnONPs).

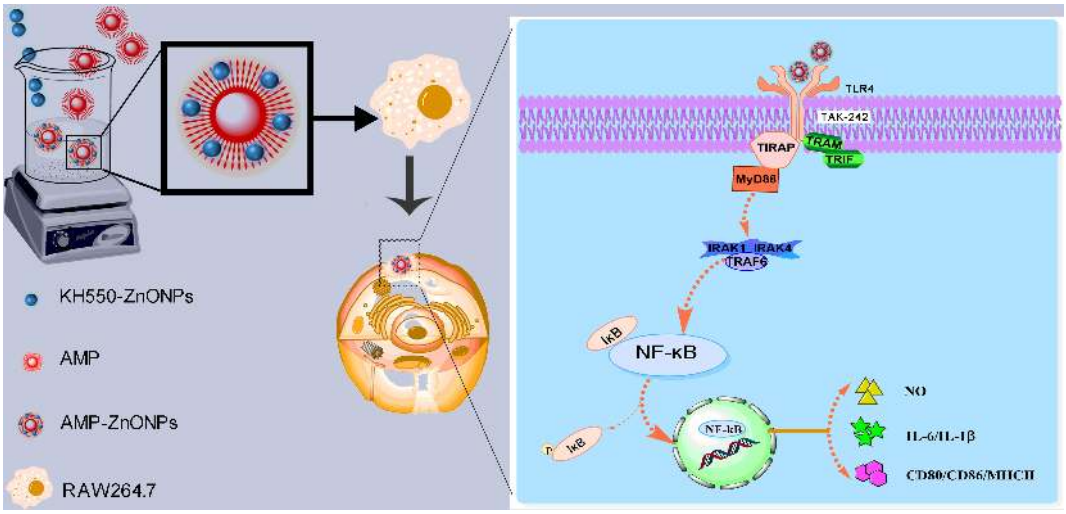

FIGURE 10
Schematic illustration depicts that a new approach was carried out to bind AMP with ZnONPs as an immunostimulator. AMP-ZnONPs could significantly activate RAW264.7 cells by TLR4/MyD88/NF-κB signaling pathway to improve its immune function. Therefore, AMP-ZnONPs remarkably enhanced phagocytosis, the release of NO, cytokines and the costimulatory molecules of RAW264.7 cells.

AMP-ZnONPs induced cells morphological changes

Macrophages engulf nutrients and pathogens by stretching their arms (59). The morphology was observed by SEM as shown in **Figure 8E**. Cells in the control group had a round shape and microvilli-like structures on the cell surface. RAW264.7 cells showed elongated and polygonal with many filopodia in the LPS group than in the other groups. In the AMP-ZnONPs group, even in the case of round-shaped RAW264.7 cells, their arms were stretching in various directions. The size, microvilli-like structures and surface folds of the AMP-ZnONPs treated group were more than ZnONPs and AMP. These results indicated that AMP-ZnONPs could induce RAW264.7 cells activation visibly, which was inconsistent with the results of phagocytosis and cytokine secretion.

AMP-ZnONPs regulated the expression of TLR4/MyD88/NF-κB associated proteins

As an important member of the TLR family, TLR4 has been widely reported to recognize and bind to different pathogen-related molecular patterns, initiate intracellular signal transduction pathways, cause the release of cytokines or

chemokines, and play an effective innate immune response (60). Whether AMP-ZnONPs could mediate the immunomodulatory effect on RAW264.7 cells by the TLR4 signaling pathway was explored. The RT-qPCR and Western blot were used to detect the mRNA and proteins of key nodes in the TLR4/MyD88/NF-κB signaling pathways. As shown in **Figures 9A,B**, compared with AMP group, the protein expression levels of TLR4, MyD88, TRAF6, P-IκBα and P-p65 were upregulated in AMP-ZnONPs group. As shown in **Figure 9C**, AMP-ZnONPs significantly up-regulated the mRNA expression of TLR4, MyD88, TRAF6 in the RAW264.7 cells, compared with those in control, ZnONPs and AMP group. Therefore, the results indicated that AMP-ZnONPs was more effective than ZnONPs and AMP in activating the TLR4/MyD88/NF-κB signaling pathway.

AMP-ZnONPs downregulated expression of TLR4/MyD88/NF-κB associated proteins after treating with the TLR4 blocker TAK242

TAK242 is a specific inhibitor of TLR4 that affects the downstream signal transduction of TLR4 by interfering with the intracellular segment of TLR4 (61). In order to further verify that AMP-ZnONPs could activate the TLR4/MyD88/NF-κB signaling pathway, RAW264.7 cells were treated with the TLR4 antagonist TAK242, and the expression of key proteins in the pathway were detected. After adding TAK242, the expression of each protein in the TLR4 pathway was shown in **Figure 9D**. Compared with the control group, the expression of TLR4, MyD88, TRAF6, P-IκBα and P-p65 were increased after treatment with AMP-ZnONPs (**Figure 9B**), while the expression of the above proteins was significantly reduced after TAK242 was added (**Figure 9E**).

TLR4 generally signals *via* a MyD88-dependent pathway, then IKK phosphorylates IκB and p65 resulting in degradation of IκB and activation of NF-κB, a nuclear factor that is responsible for the production of many cytokines (IL-6, IL-1β) and the costimulatory molecules (CD80, CD86, MHCII). In this study, AMP-ZnONPs could significantly activate RAW264.7 cells by TLR4/MyD88/NF-κB signaling pathway to improve its immune function. TAK242, a specific TLR4 inhibitor, reversely demonstrated that AMP-ZnONPs could promote the expression of TLR4 pathway-related proteins. In conclusion, this study can provide a new research idea for the development and utilization of polysaccharides and microelements in the food and pharmaceutical industry and presents a theoretical basis for research and development into new immunomodulatory nutraceutical or immune adjuvant (**Figure 10**).

Conclusion

In summary, by Borch reaction between AMP and ZnONPs modified by KH550, the AMP-ZnONPs was successfully prepared and its characterization was evaluated. AMP-ZnONPs showed excellent immunostimulatory activity on macrophages and the activities were much better than those of ZnONPs or AMP applied alone. Furthermore, this study clarified that AMP-ZnONPs could significantly activate RAW264.7 cells by TLR4/MyD88/NF-κB signaling pathway to improve its immune function. These data demonstrated that AMP binding with ZnONPs could potentially be used as an easily available source for immunomodulatory nutraceutical or immune adjuvant, which can be widely used in the food or medicine industry in the future.

Data availability statement

The datasets presented in this study can be found in online repositories. The names of the repository/repositories and accession number(s) can be found in the article/supplementary material.

Author contributions

RB: conceptualization, methodology, software, data curation, writing—original draft, review and editing, visualization, supervision, project administration, and funding acquisition. XL: conceptualization, methodology, investigation, software, data curation, writing—original draft, and visualization. JW: methodology, investigation, and software. SW: investigation and writing—review and editing. XW: investigation and software. YT and SX: visualization and investigation. ML: supervision. JL: conceptualization, methodology, project administration, and funding acquisition. HP: conceptualization and methodology. All authors contributed to the article and approved the submitted version.

Funding

This work was supported by the Natural Science Foundation of Jiangsu Province (Grant no. BK2020945), the National Natural Science Foundation of China (Grant nos. 32002324, 32072911, and U1904215), the China Postdoctoral Science Foundation (Grant no. 2021M692716), Postgraduate Research and Practice Innovation Program of Jiangsu Province (No. SJCX22-1806), and the Priority Academic Program Development of Jiangsu Higher Education Institutions (PAPD).

Conflict of interest

The authors declare that the research was conducted in the absence of any commercial or financial relationships that could be construed as a potential conflict of interest.

Publisher's note

All claims expressed in this article are solely those of the authors and do not necessarily represent those of their affiliated organizations, or those of the publisher, the editors and the reviewers. Any product that may be evaluated in this article, or claim that may be made by its manufacturer, is not guaranteed or endorsed by the publisher.

References

1. Yun C, Yao F, Ke M, Wang D, Hu Y, Liu J. Polysaccharides from traditional chinese medicines: Extraction, purification, modification, and biological activity. *Molecules.* (2016) 21:1705. doi: 10.3390/molecules21121705

2. Qin J, Wang HY, Zhuang D, Meng FC, Lv GP. Structural characterization and immunoregulatory activity of two polysaccharides from the rhizomes of *Atractylodes lancea* (thunb.) dc. *Int J Biol Macromol.* (2019) 136:341–51. doi: 10.1016/j.ijbiomac.2019.06.088

3. Wang P, Zhao YN, Xu RZ, Zhang XW, Sun YR, Feng QM, et al. Sesquiterpene Lactams and Lactones With Antioxidant Potentials From *Atractylodes macrocephala* Discovered by Molecular Networking Strategy. *Front Nutr.* (2022) 9:865257. doi: 10.3389/fnut.2022.865257

4. Li J, Hu D, Zong W, Lv G, Zhao J, Li S. Determination of inulin-type fructooligosaccharides in edible plants by high-performance liquid chromatography with charged aerosol detector. *J Agr Food Chem.* (2014) 62:7707–13. doi: 10.1021/jf502329n

5. Chau CF, Wu SH. The development of regulations of Chinese herbal medicines for both medicinal and food uses. *Trends Food Sci Tech.* (2006) 17:313–23. doi: 10.1016/j.tifs.2005.12.005

6. Sun W, Meng K, Qi C, Yang X, Wang Y, Fan W, et al. Immune-enhancing activity of polysaccharides isolated from *Atractylodis macrocephalae* Koidz. *Carbohydr Polym.* (2015) 126:91–6. doi: 10.1016/j.carbpol.2015.03.034

7. Xu W, Fang S, Wang Y, Chi X, Ma X, Zhang T, et al. Receptor and signaling pathway involved in bovine lymphocyte activation by *Atractylodis macrocephalae* polysaccharides. *Carbohyd Polym.* (2020) 234:115906. doi: 10.1016/j.carbpol.2020.115906

8. Xue W, Gao Y, Li Q, Lu Q, Bian ZY, Tang L, et al. Immunomodulatory activity-guided isolation and characterization of a novel polysaccharide from *Atractylodis macrocephalae* Koidz. *Int J Biol Macromol.* (2020) 161:514–24. doi: 10.1016/j.ijbiomac.2020.06.003

9. Zhu S, Sun Y, Jia Y, Zhang W, Wang Y, Li L, et al. Acid site-regulated solid acids for polysaccharide se-functionalization: Structural explanations for high reactivity. *Carbohydr Polym.* (2020) 251:117028. doi: 10.1016/j.carbpol.2020.117028

10. Satyavathi CT, Tomar RS, Ambawat S, Kheni J, Padhiyar SM, Desai H, et al. Stage specific comparative transcriptomic analysis to reveal gene networks regulating iron and zinc content in pearl millet [*Pennisetum glaucum* (L.) R. Br.]. *Sci Rep.* (2022) 12:276. doi: 10.1038/s41598-021-04388-0

11. Sandek A, Doehner W, Anker SD, Haehling S. Nutrition in heart failure: an update. *Curr Opin Clin Nutr Metab Care.* (2009) 12:384–91. doi: 10.1097/MCO.0b013e32832cdb0f

12. Alam S, Kelleher SL. Cellular mechanisms of zinc dysregulation: a perspective on zinc homeostasis as an etiological factor in the development and progression of breast cancer. *Nutrients.* (2012) 4:875–903. doi: 10.3390/nu4080875

13. Vaikundamoorthy R, Hwang I. Zinc oxide nanoparticles promoting the formation of myogenic differentiation into myotubes in mouse myoblast C2C12 cells. *J Ind and Eng Chem.* (2020) 83:315–22. doi: 10.1016/j.jiec.2019.12.004

14. Cunnane SC. Foetal mortality in moderately zinc-deficient rats is strictly related to the process of parturition: effect of maternal essential fatty acid supplementation. *Br J Nutr.* (1982) 47:495–504. doi: 10.1079/BJN19820062

15. Li J, Chen H, Bing W, Cai C, Xu Y, Chai Z, et al. ZnO nanoparticles act as supportive therapy in DSS-induced ulcerative colitis in mice by maintaining gut homeostasis and activating NrF2 signaling. *Sci Rep.* (2017) 7:43126. doi: 10.1038/srep43126

16. Name JJ, Souza ACR, Vasconcelos AR, Prado PS, Pereira CPM. Zinc, Vitamin D and Vitamin C: Perspectives for COVID-19 With a Focus on Physical Tissue Barrier Integrity. *Front Nutr.* (2020) 7:606398. doi: 10.3389/fnut.2020.606398

17. Maares M, Haase H. Zinc and immunity: An essential interrelation. *Arch Biochem Biophys.* (2016) 611:58–65. doi: 10.1016/j.abb.2016.03.022

18. Maywald M, Wessels I, Rink L. Zinc Signals and Immunity. *Int J Mol Sci.* (2017) 18:2222. doi: 10.3390/ijms18102222

19. Meng S, Hong Y, Dai Z, Huang W, Dong X. Simultaneous detection of dihydroxybenzene isomers with ZnO nanorod/carbon cloth electrodes. *ACS Appl Mater Interfaces.* (2017) 9:12453–60. doi: 10.1021/acsami.7b00546

20. Tanino R, Amano Y, Tong X, Sun R, Isobe T. Anticancer activity of ZnO nanoparticles against human small-cell lung cancer in an orthotopic mouse model. *Mol Cancer Ther.* (2019) 19:502–12. doi: 10.1158/1535-7163.MCT-19-0018

21. Webster T, Maschhoff P, Geilich B. Greater fibroblast proliferation on an ultrasonicated ZnO/PVC nanocomposite material. *Int J Nanomed.* (2013) 9:257–63. doi: 10.2147/IJN.S54897

22. Becker L, Gharib SA, Irwin AD, Wijsman E, Vaisar T, Oram JF, et al. A macrophage sterol-responsive network linked to atherogenesis. *Cell Metab.* (2010) 11:125–35. doi: 10.1016/j.cmet.2010.01.003

23. Yang X, Zhou S, Li H, An J, Li C, Zhou R, et al. Structural characterization of alpiniae oxyphyllae fructus polysaccharide 2 and its activation effects on RAW264.7 macrophages. *Int Immunopharmacol.* (2021) 97:107708. doi: 10.1016/j.intimp.2021.107708

24. Zhou R, Teng L, Zhu Y, Zhang C, Yang Y, Chen Y. Preparation of Amomum longiligulare polysaccharides 1- PLGA nanoparticle and its immune enhancement ability on RAW264.7 cells. *Int Immunopharmacol.* (2021) 99:108053. doi: 10.1016/j.intimp.2021.108053

25. Zhu L, Wei L, Fan Z, Ye X, Lin R, Ban M, et al. Immunomodulatory activity of polysaccharide from *Arca granosa* Linnaeus via TLR4/MyD88/NFκB and TLR4/TRIF signaling pathways. *J Funct Foods.* (2021) 84:104579. doi: 10.1016/j.jff.2021.104579

26. Chen Y, Zhou R, He L, Wang F, Chen H. Okra polysaccharide-2 plays a vital role on the activation of RAW264.7 cells by TLR2/4-mediated signal transduction pathways. *Int Immunopharmacol.* (2020) 86:106708. doi: 10.1016/j.intimp.2020.106708

27. Xu Z, Lin R, Hou X, Wu J, Zhao W, Ma H, et al. Immunomodulatory mechanism of a purified polysaccharide isolated from isaria cicadae miquel on RAW264.7 cells via activating TLR4-MAPK-NF-κB signaling pathway. *Int J Biol Macromol.* (2020) 164:4329–38. doi: 10.1016/j.ijbiomac.2020.09.035

28. Zhang M, Yan M, Yang J, Li F, Wang Y, Feng K, et al. Structural characterization of a polysaccharide from *Trametes sanguinea* Lloyd with immune-enhancing activity via activation of TLR4. *Int J Biol Macromol.* (2022) 206:1026–38. doi: 10.1016/j.ijbiomac.2022.03.072

29. Xie Y, Wang L, Sun H, Wang Y, Yang Z, Zhang G, et al. Polysaccharide from alfalfa activates RAW264.7 macrophages through MAPK and NF-κB signaling pathways. *Int J Biol Macromol.* (2019) 126:960–8. doi: 10.1016/j.ijbiomac

30. Xiong L, Ouyang KH, Jiang Y, Yang ZW, Hu WB, Chen H, et al. Chemical composition of *Cyclocarya paliurus* polysaccharide and inflammatory effects in lipopolysaccharide-stimulated RAW264.7 macrophage. *Int J Biol Macromol.* (2018) 107:1898–907. doi: 10.1016/j.ijbiomac.2017.10.055

31. Qin T, Liu X, Luo Y, Yu R, Chen S, Zhang J, et al. Characterization of polysaccharides isolated from *Hericium erinaceus* and their protective effects on the don-induced oxidative stress. *Int J Biol Macromol.* (2020) 152:1265–73. doi: 10.1016/j.ijbiomac.2019.10.223

32. Liu M, Zhang C, Xu X, Zhao X, Han Z, Liu D, et al. Ferulic acid inhibits LPS-induced apoptosis in bovine mammary epithelial cells by regulating the NF-κB and Nrf2 signalling pathways to restore mitochondrial dynamics and ROS generation. *Vet Res.* (2021) 52:104. doi: 10.1186/s13567-021-00973-3

33. Zhu Y, Huang Y, Yang J, Tu R, Zhang X, He WW, et al. Intranasal insulin ameliorates neurological impairment after intracerebral hemorrhage in mice. *Neural Regen Res.* (2021) 17:210–6. doi: 10.4103/1673-5374.314320

34. Liu X, Ren Z, Yu R, Chen S, Zhang J, Xu Y, et al. Structural characterization of enzymatic modification of *Hericium erinaceus* polysaccharide and its immune-enhancement activity. *Int J Biol Macromol.* (2021) 166:1396–408. doi: 10.1016/j.ijbiomac.2020.11.019

35. Feng YY, Ji HY, Dong XD, Liu AJ. An alcohol-soluble polysaccharide from *Atractylodes macrocephala* koidz induces apoptosis of Eca-109 cells. *Carbohyd Polym.* (2019) 226:115136. doi: 10.1016/j.carbpol.2019.115136

36. Yu-Hao D, Chun C, Xiong F, Rui L. Study on the pharmacokinetics of mulberry fruit polysaccharides through fluorescence labeling. *Int J Biol Macromol.* (2021) 186:462–71. doi: 10.1016/j.ijbiomac.2021.07.075

37. Hong RY, Li JH, Chen LL, Liu DQ, Li HZ, Zheng Y, et al. Synthesis, surface modification and photocatalytic property of ZnO nanoparticles. *Powder Technol.* (2009) 189:426–32. doi: 10.1016/j.powtec.2008.07.004

38. Du GX, Xue Q, Ding H, Li Z. Mechanochemical effects of ZnO powder in a wet super-fine grinding system as indicated by instrumental characterization. *Int J Miner Proc.* (2015) 141:15–9. doi: 10.1016/j.minpro.2015.06.008

39. Qiao Y, Li W, Bao J, Zheng Y, Feng L, Ma Y, et al. Controlled synthesis and luminescence properties of core-shell-shell structured SiO2@AIPA-S-Si-Eu@SiO2 and SiO2@AIPA-S-Si-Eu-phen@SiO2 nanocomposites. *Sci Rep.* (2020) 10:3522. doi: 10.1038/s41598-020-60538-w

40. Pawar S, Shende P. 22 factorial design-based biocompatible microneedle arrays containing artemether co-loaded with lumefantrine nanoparticles for transepidermal delivery. *Biomed Microdevices.* (2020) 22:19. doi: 10.1007/s10544-020-0476-8

41. Hawash MM, Kahraman DC, Eren F, Cetin Atalay R, Baytas SN. Synthesis and biological evaluation of novel pyrazolic chalcone derivatives as novel hepatocellular carcinoma therapeutics. *Eur J Med Chem.* (2017) 129:12–26. doi: 10.1016/j.ejmech.2017.02.002

42. Ding Y, Sun H, Ren C, Zhang M, Sun K. A nonenzymatic glucose sensor platform based on specific recognition and conductive polymer-decorated CuCo2O4 carbon nanofibers. *Materials.* (2020) 13:2874. doi: 10.3390/ma13122874

43. Ji X, Hou C, Yan Y, Shi M, Liu Y. Comparison of structural characterization and antioxidant activity of polysaccharides from jujube (*ziziphus jujuba* mill.) fruit. *Int J Biol Macromol.* (2020) 149:1008–18. doi: 10.1016/j.ijbiomac.2020.02.018

44. Suvakanta D, Narsimha MP, Pulak D, Joshabir C, Biswajir D. Optimization and characterization of purified polysaccharide from musa sapientum l. as a pharmaceutical excipient. *Food Chem.* (2014) 149:76–83. doi: 10.1016/j.foodchem.2013.10.068

45. Copperthwaite RG, Kunze OA, Lloyd J, Neely JA, Tuma W. Surface analysis of insb by x-ray photoelectron spectroscopy (XPS). *Z Naturforsch A.* (1978) 33:523–7. doi: 10.1515/zna-1978-0503

46. Ding Z, Wang L, Xing Y, Zhao Y, Han J. Enhanced oral bioavailability of celecoxib nanocrystalline solid dispersion based on wet media milling technique: formulation, optimization and in vitro/in vivo evaluation. *Pharmaceutics.* (2019) 11:328. doi: 10.3390/pharmaceutics11070328

47. Liu X, Xie J, Jia S, Huang L, Wang Z, Li C, et al. Immunomodulatory effects of an acetylated *Cyclocarya paliurus* polysaccharide on murine macrophages RAW264.7. *Int J Biol Macromol.* (2017) 98:576–81. doi: 10.1016/j.ijbiomac.2017.02.028

48. Zhang M, Tian X, Wang Y, Wang D, Li W, Chen L, et al. Immunomodulating activity of the polysaccharide TLH-3 from tricholomalobayense in RAW264.7 macrophages. *Int J Biol Macromol.* (2017) 107:2678–85. doi: 10.1016/j.ijbiomac.2017.10.165

49. Guo G, Gong T, Shen H, Wang Q, Jiang F, Tang J, et al. Self-amplification immunomodulatory strategy for tissue regeneration in diabetes based on cytokine-zifs system. *Adv Funct Mater.* (2021) 31:2100795. doi: 10.1002/adfm.202100795

50. Srinivasan A, Ekambaram S, Selvan PS. Plant polysaccharides-An insight into its immunostimulatory properties. *Bioact Carbohydr Diet.* (2021) 25:100244. doi: 10.1016/j.bcdf.2020.100244

51. Yoo HG, Shin BA, Park JS, Lee KH, Jung YD. IL-1beta induces MMP-9 via reactive oxygen species and NF-kappaB in murine macrophage RAW264.7 cells. *Biochem Biophys Res Commun.* (2002) 298:251–6. doi: 10.1016/S0006-291X(02)02431-2

52. Wufuer R, Bai J, Liu Z, Zhou K, Taoerdahong H. Biological activity of *Brassica rapa* L. polysaccharides on RAW264.7 macrophages and on tumor cells-ScienceDirect. *Bioorg Med Chem.* (2020) 28:115330. doi: 10.1016/j.bmc.2020.115330

53. Qian JY, Chen W, Zhang WM, Hao Z. Adulteration identification of some fungal polysaccharides with sem, xrd, ir and optical rotation: A primary approach. *Carbohyd Polym.* (2009) 78:620–5. doi: 10.1016/j.carbpol.2009.05.025

54. Cui F, Jiang L, Qian L, Sun W, Tao T, Zan X, et al. A macromolecular α-glucan from fruiting bodies of Volvariella volvacea activating RAW264.7 macrophages through MAPKs pathway. *Carbohydr Polym.* (2020) 230:115674. doi: 10.1016/j.carbpol.2019.115674

55. Zhang H, Li C, Lai PFH, Chen J, Ai L. Fractionation, chemical characterization and immunostimulatory activity of β-glucan and galactoglucan from *Russula vinosa* Lindblad. *Carbohydr Polym.* (2021) 256:117559. doi: 10.1016/j.carbpol.2020.117559

56. Zhang M, Zhao M, Qing Y, Luo Y, Xia G, Li Y. Study on immunostimulatory activity and extraction process optimization of polysaccharides from *Caulerpa lentillifera*. *Int J Biol Macromol.* (2020) 143:677–84. doi: 10.1016/j.ijbiomac.2019.10.042

57. Li X, Xing R, Xu C, Liu S, Qin Y, Li K, et al. Immunostimulatory effect of chitosan and quaternary chitosan: A review of potential vaccine adjuvants. *Carbohydr Polym.* (2021) 264:118050. doi: 10.1016/j.carbpol.2021.118050

58. Cobb BA, Wang Q, Tzianabos AO, Kasper DL. Polysaccharide processing and presentation by the MHCII pathway. *Cell.* (2004) 117:677–87. doi: 10.1016/j.cell.2004.05.001

59. Zong L, Zhang J, Dai L, Liu J, Yang Y, Xie J, et al. The Anti-Inflammatory Properties of Rhododendron molle Leaf Extract in LPS-Induced RAW264.7. *Chem Biodivers.* (2020) 17:e2000477. doi: 10.1002/cbdv.202000477

60. Liu Y, Yin H, Zhao M, Lu Q. TLR2 and TLR4 in autoimmune diseases: a comprehensive review. *Clin Rev Allergy Immunol.* (2014) 47:136–47. doi: 10.1007/s12016-013-8402-y

61. Engelmann C, Sheikh M, Sharma S, Kondo T, Loeffler-Wirth H, Zheng YB, et al. Toll-like receptor 4 is a therapeutic target for prevention and treatment of liver failure. *J Hepatol.* (2020) 73:102–12. doi: 10.1016/j.jhep.2020.01.011